

# Ferromagnetism in two-dimensional CrTe<sub>2</sub> epitaxial films down to a few atomic layers



Cite as: AIP Advances 11, 035138 (2021); doi: 10.1063/5.0041531

Submitted: 30 January 2021 • Accepted: 16 February 2021 •

Published Online: 23 March 2021



View Online



Export Citation



CrossMark

Yizhe Sun,<sup>1</sup> Pengfei Yan,<sup>1</sup> Jiai Ning,<sup>1</sup> Xiaoqian Zhang,<sup>1</sup> Yafei Zhao,<sup>1</sup> Qinwu Gao,<sup>1</sup> Moorthi Kanagaraj,<sup>1</sup> Kunpeng Zhang,<sup>2</sup> Jingjing Li,<sup>3</sup> Xianyang Lu,<sup>1</sup> Yu Yan,<sup>1</sup> Yao Li,<sup>1,4</sup> Yongbing Xu,<sup>1,2,4</sup> and Liang He<sup>1,4,a)</sup>

## AFFILIATIONS

<sup>1</sup>National Laboratory of Solid State Microstructures and Jiangsu Provincial Key Laboratory of Advanced Photonic and Electronic Materials, School of Electronic Science and Engineering, Nanjing University, Nanjing 210093, China

<sup>2</sup>Nanjing-York Joint Center of Spintronics and NanoEngineering and Department of Physics, The University of York, York YO105DD, United Kingdom

<sup>3</sup>School of Art and Design, Chuzhou University, Chuzhou 239000, China

<sup>4</sup>Collaborative Innovation Center of Advanced Microstructures, Nanjing University, Nanjing 210093, China

<sup>a)</sup>Author to whom correspondence should be addressed: [heliang@nju.edu.cn](mailto:heliang@nju.edu.cn)

## ABSTRACT

Two-dimensional (2D) van der Waals ferromagnetic materials have attracted intense attention due to their potential impact on both fundamental and applied research studies. Recently, a new 2D ferromagnet CrTe<sub>2</sub>, prepared by mechanical exfoliation or chemical vapor deposition, has gained interest due to its novel magnetic properties. In this work, high quality CrTe<sub>2</sub> epitaxial thin films were prepared on GaAs (111)B substrates using solid source molecular beam epitaxy, with the thickness varying from 35 to 4 monolayers (MLs). The magnetic easy axis of all the films is oriented along the c-axis. A Curie temperature of 205 K is found in the 35 ML CrTe<sub>2</sub> film, measured by the temperature-dependent anomalous Hall resistance ( $R_{AHE}$ ). Importantly, even when the film thickness decreases to 4 MLs, a robust **out-of-plane ferromagnetism** with a **Curie temperature of 191 K** has been demonstrated. This finding could pave the way for investigating the fundamental studies in 2D ferromagnetism and has great significance in device applications.

© 2021 Author(s). All article content, except where otherwise noted, is licensed under a Creative Commons Attribution (CC BY) license (<http://creativecommons.org/licenses/by/4.0/>). <https://doi.org/10.1063/5.0041531>

Atomically thin two-dimensional (2D) van der Waals (vdW) materials have attracted extensive attention<sup>1</sup> owing to their remarkable properties in diverse experimental fields, such as electronics,<sup>2,3</sup> optoelectronics,<sup>4–6</sup> magnetism,<sup>7</sup> thermoelectrics,<sup>8</sup> and spintronic devices.<sup>9</sup> Among these, intrinsic 2D magnetic materials, such as CrI<sub>3</sub>,<sup>10</sup> Fe<sub>3</sub>GeTe<sub>2</sub>,<sup>11,12</sup> and Cr<sub>2</sub>Ge<sub>2</sub>Te<sub>6</sub>,<sup>13</sup> have aroused great interest not only due to their fascinating magnetic properties in the 2D limit but also for opening new avenues for applications in spintronics.<sup>13–15</sup> Recently, a new 2D ferromagnetic material CrTe<sub>2</sub> has been found.<sup>16,17</sup> Freitas *et al.* reported that they had synthesized the metastable compound 1T-CrTe<sub>2</sub> for the first time.<sup>16</sup> Purbawati *et al.* reported thin CrTe<sub>2</sub> flakes with a T<sub>c</sub> above room temperature.<sup>18</sup> Sun *et al.* found that the ferromagnetism could hold above room temperature in a metallic phase of 1T-CrTe<sub>2</sub> down to the ultra-thin limit.<sup>19</sup> However, all of the reported CrTe<sub>2</sub> are prepared in bulk forms, and the devices are made by mechanical exfoliation and stacking techniques.<sup>12,19–21</sup> The size and thickness of 2D materials obtained by

exfoliation are uncontrolled, which prevents them being applied in actual production. Thus, the preparation of the large-scale samples with high quality is of great significance.

In this work, a series of CrTe<sub>2</sub> thin films with various thicknesses from 35 to 4 monolayers (MLs) were epitaxially grown on high resistivity ( $\approx 10 \text{ M}\Omega \text{ cm}$ ) GaAs (111)B substrates using molecular beam epitaxy (MBE). The base pressure of the growth chamber is below  $2 \times 10^{-10} \text{ Torr}$ . The GaAs (111)B substrates were cleaned under a standard procedure before being loaded into the chamber.<sup>22</sup> Then, the substrates were annealed at 580 °C in the growth chamber until the streak patterns appeared as monitored by the real-time RHEED,<sup>23</sup> as shown in Fig. 1(b). High-purity Cr (99.999%) and Te (99.9999%) were evaporated by conventional effusion cells. During the growth, the Cr effusion cell was kept at 1180 °C and the Te effusion cell was kept at 255 °C to keep the flux ratio of Cr/Te at 1/20 to maintain a Te-rich environment. The GaAs (111)B substrates were set at 265 °C during the growth for all the samples.

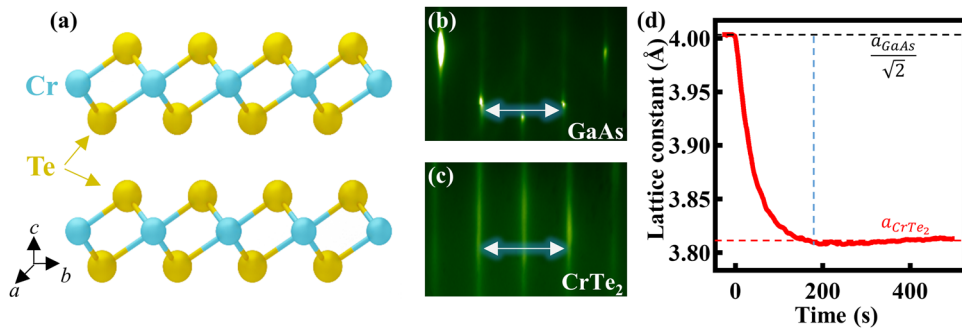
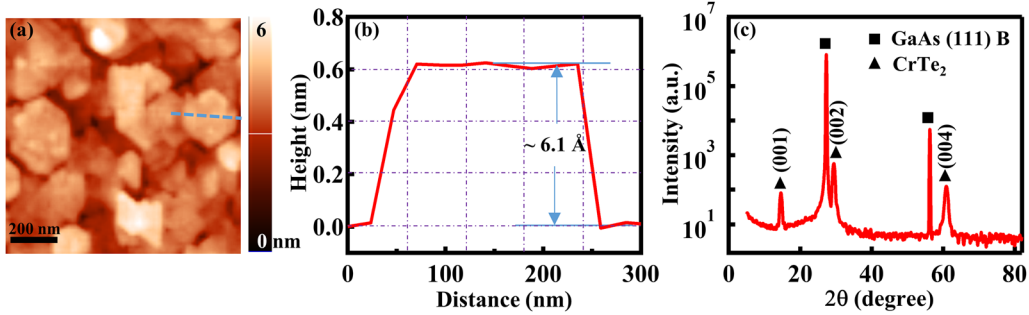


**FIG. 1.** (a) Schematics of the crystal structure of CrTe<sub>2</sub>. The RHEED patterns of the GaAs (111)B substrate (b) and a CrTe<sub>2</sub> thin film (c), respectively. The double-headed arrows between the two first order stripes represent the *d*-spacing, which is inversely proportional to the in-plane lattice constant. (d) The time evolution of the lattice constant of the film during growth. The black horizontal and red dashed lines indicate the lattice constant of the GaAs (111)B substrate and CrTe<sub>2</sub> film, respectively. The blue dashed line shows the finishing time of the first ML.

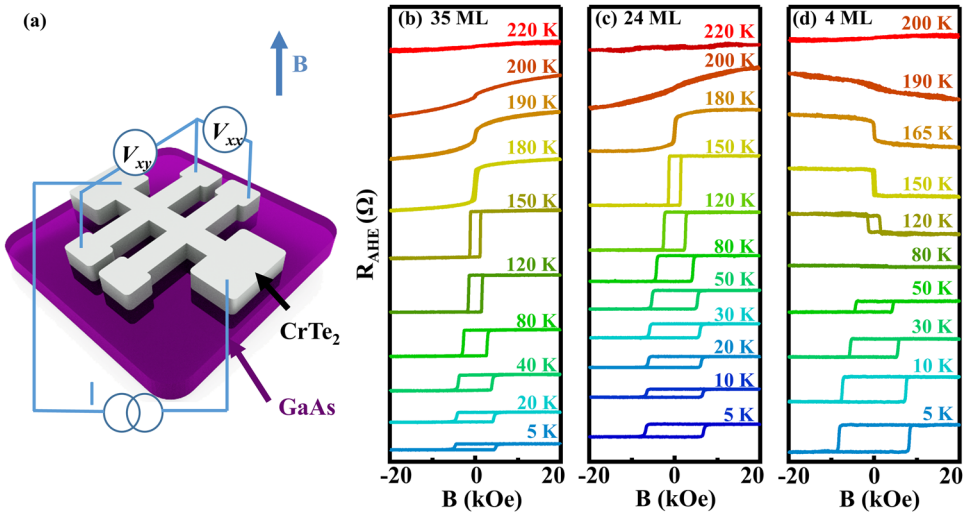
Figure 1(a) presents the crystalline structure of the CrTe<sub>2</sub> compound. They crystallize in the space group of  $\bar{p}\bar{3}m1$ , with the layered structures stacked by the Te–Cr–Te sandwich layers along the *c* axis,<sup>18</sup> while between the layers, the interactions are mainly of the van der Waals type.<sup>24</sup> Figures 1(b) and 1(c) show representative RHEED patterns of the GaAs (111)B substrate and the CrTe<sub>2</sub>, respectively. Sharp streaky patterns were observed after growth, which indicates the flat surface morphology of the films. The double-headed arrows between the two first order stripes represent the *d*-spacing,<sup>25</sup> which is inversely proportional to the in-plane lattice constant. For GaAs (111)B, the atoms are close-packed in the (111) plane, which makes its in-plane lattice constant to be  $a_{\text{GaAs}}/\sqrt{2}$  of  $\sim 4.0 \text{ \AA}$ , as shown by the black dashed line in Fig. 1(d). From this, the lattice constant of the films can be extracted to be  $3.81 \text{ \AA}$ , which is very close to the theoretical value of  $3.79 \text{ \AA}$ ,<sup>18,26</sup> as shown by the red dashed line in Fig. 1(d). Figure 1(d) illustrates the evolution of the lattice constant of CrTe<sub>2</sub> film during growth. Soon after the beginning of the growth, the lattice constant of the film decreases from the GaAs substrates and reaches CrTe<sub>2</sub> after the first layer, as indicated by the blue dashed line. This suggests that the films have completely released the strain from the substrate after the growth of the first layer, which is consistent with the van der Waals epitaxial growth mode.<sup>27</sup>

Figure 2(a) shows a typical atomic force microscopy (AFM) (NT-MDT, INTEGRA SPECTRA II, Probe aperture size  $\sim 100 \text{ nm}$ ) image of an as-grown CrTe<sub>2</sub> film. Hexagonal terraces can be observed with a typical size of  $\sim 200 \text{ nm}$ , reflecting the hexagonal crystal structure inside the (0001) plane.<sup>28</sup> Figure 2(b) displays the height profile of the dashed line in Fig. 2(a). The height is equal to  $\sim 6.1 \text{ \AA}$ , consistent with a CrTe<sub>2</sub> ML thickness.<sup>16,26</sup> The phase purity and crystal structure of the CrTe<sub>2</sub> thin film have been identified by x-ray diffraction (Bruker D8 Discover single crystal diffractometer,  $\lambda = 1.5406 \text{ \AA}$ ) and the spectra are shown in Fig. 2(c). Compared with the Joint Committee on Powder Diffraction Standards (JCPDS) data of CrTe<sub>2</sub>, the film has been found to exhibit rhombohedral crystal geometry with no other detectable phases.<sup>24</sup> The lattice parameter *c* was calculated as  $6.144 \text{ \AA}$  according to the position of the XRD peaks, which is consistent with the value of  $6.166 \text{ \AA}$  by the theoretical calculation.<sup>19,24</sup>

After growth, the samples are patterned into standard Hall bar devices using Ion Beam Etching (IBE) with Ar gas. The magnetic properties of the samples were examined by the magneto-transport measurements inside an Oxford instruments' cryogenic system (TeslatronPT), as shown in Fig. 3(a). A Keithley 6221 AC/DC current source was used to apply an AC of  $1 \mu\text{A}$  with a frequency of 13 Hz. Lock-in amplifier SR830 was employed to obtain the



**FIG. 2.** (a) A typical AFM image of an as-grown CrTe<sub>2</sub> film. (b) The height profile along the dashed line in (a) demonstrates that the terrace height is  $\sim 6.1 \text{ \AA}$ , about one CrTe<sub>2</sub> layer. (c) XRD pattern of a 35 ML CrTe<sub>2</sub> thin film.



**FIG. 3.** (a) A schematic diagram of the CrTe<sub>2</sub> (white) on a highly resistive GaAs (111)B (purple) Hall bar device with the measurement setup. Anomalous Hall resistance,  $R_{AHE} = R_{xy} - R_0 H$ , of the 35 (b), 24 (c), and 4 ML (d) CrTe<sub>2</sub> film vs magnetic field at various temperatures.

longitudinal and transverse voltage signals, while the magnetic field up to 2 T was scanned back and forth perpendicular to the sample surface.

Generally, there is a close correlation between magnetism and transport in magnetic materials, and the anomalous Hall effect (AHE) is utilized to demonstrate the prevailing ferromagnetism. The Hall resistance ( $R_{xy}$ ) follows an empirical relation<sup>29</sup>  $R_{xy} = R_0 H + R_{AHE}(H)$ , where the first term is the ordinary Hall effect and the second is the AHE with respective coefficients  $R_0$  and  $R_{AHE}$ . Here,  $R_0$  is the ordinary Hall coefficient and is solely connected to the carrier density, and  $R_{AHE}$  is proportional to the longitudinal resistance  $R_{xx}$  or  $R_{xx}^{-2}$  depending on the dominant extrinsic scattering mechanisms.<sup>31</sup>

By subtracting the linear ordinary Hall component  $R_0 H$ , the anomalous Hall data  $R_{AHE} = R_{xy} - R_0 H$  of 35, 24, and 4 ML CrTe<sub>2</sub> films were plotted at different temperatures in Figs. 3(b)–3(d),

respectively. For the 35 ML CrTe<sub>2</sub> film, a square hysteresis loop can be observed at low temperatures, suggesting its ferromagnetism and the out-of-plane easy axis. As the temperature rises, the saturated  $R_{AHE}$  first increases and reaches the maximum at about 150 K, then decreases, and finally disappears around 200 K, as shown in Fig. 4(a). The coercive field ( $H_c$ ) decreases and eventually vanished around 200 K. Similar behaviors are also observed in the 24 ML sample, as shown in Fig. 3(c).

For the 4 ML CrTe<sub>2</sub> film, as the temperature increases, the saturated  $R_{AHE}$  first decreases from positive to negative at 80 K, reaches its minimum at 150 K, then increases again, and finally disappears at around 190 K. This strange temperature dependent saturated  $R_{AHE}$ , only found at very thin samples, may be associated with the change of their intrinsic anomalous Hall coefficient, which is related to their Berry curvatures.<sup>32</sup> On the other hand, its coercive field ( $H_c$ )

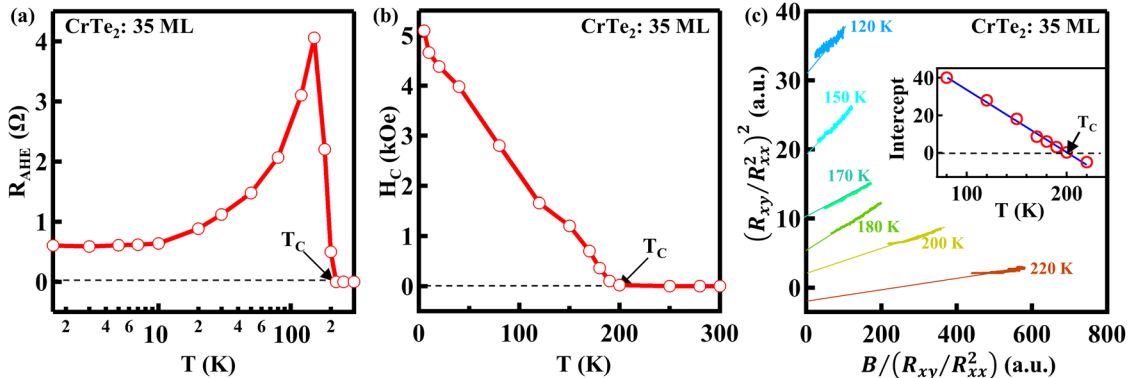


**FIG. 4.** (a) The saturated  $R_{AHE}$  vs temperature of the 35 ML CrTe<sub>2</sub>. The Curie temperature can be determined as  $\sim 202$  K. (b) The  $H_c$  vs temperature of the 35 ML CrTe<sub>2</sub>. The Curie temperature can be determined as  $\sim 203$  K. (c) Arrott-plot using anomalous Hall data at temperatures from 120 K to 220 K. The lines in different colors represent the linear fits at high fields where the magnetization is saturated. (Inset) The intercepts in the y-axis vs temperatures. The linear fit gives the Curie temperature of  $204.6 \pm 0.8$  K.

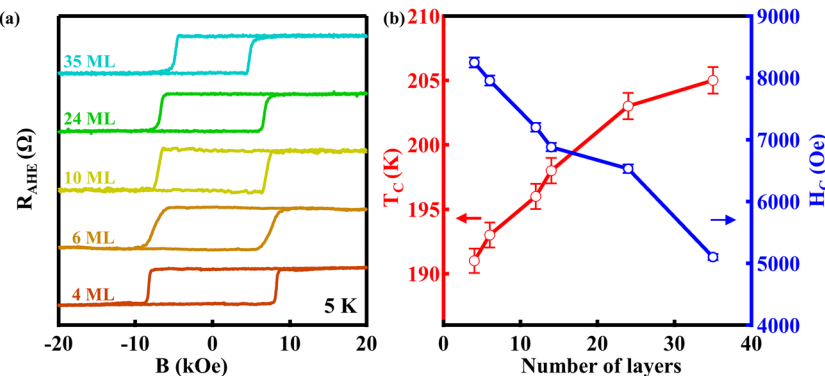


**FIG. 5.** (a) Magnetic field dependent anomalous Hall effect ( $R_{AHE}$ ) with different CrTe<sub>2</sub> thicknesses. (b) The evolution of the Curie temperature  $T_C$  (red) and the coercive field  $H_C$  (blue) at 5 K vs CrTe<sub>2</sub> thicknesses. The Curie temperature raises with the increasing film thicknesses, while the coercivity correspondingly decreases.

decreases monotonically with the increased temperature and reaches zero at 191 K.

The temperature dependent saturated  $R_{AHE}$  of the 35 ML CrTe<sub>2</sub> is plotted in Fig. 4(a), and the Curie temperature of 202 K can be determined as it reaches zero.<sup>33</sup> Figure 4(b) shows the  $H_C$  as a function of temperature. As the temperature increases,  $H_C$  drops and reaches zero at 203 K. In addition, the method of the Arrott-plot has been adopted to further confirm the ferromagnetic transition.<sup>34</sup> Here, we take the assumption of side jump mechanism at high fields and use the ratio of  $(R_{xy}/R_{xx}^2)$  to estimate the magnetization  $M$ .<sup>35,36</sup> Thus, the Arrott-plot can be plotted as  $(R_{xy}/R_{xx}^2)^2$  against  $B/(R_{xy}/R_{xx}^2)$ , where  $B$  is magnetic induction,<sup>37</sup> as shown in Fig. 4(c). It is well known that the intercept on the y-axis of the extrapolated line at high field is positive for the ferromagnetic state and negative for the paramagnetic state.<sup>38</sup> When the intercept goes to zero, the Curie temperature  $T_C$  of  $204.6 \pm 0.8$  K can be determined,<sup>39</sup> as shown in the inset of Fig. 4(c). All three methods presented here give a consistent  $T_C$  of  $\sim 205$  K for the 35 ML CrTe<sub>2</sub> films. The  $T_C$  for all other prepared samples has been determined similarly, as shown in Fig. 5(b). It decreases from 205 to 191 K, as the film thickness decreases from 35 to 4 MLs.

Figure 5(a) presents the  $R_{AHE}$  of various CrTe<sub>2</sub> thin films at 5 K. All the samples exhibit similar square hysteresis loops, demonstrating strong ferromagnetism with an out-of-plane easy axis even for the 4 ML sample.<sup>40</sup> As shown in Fig. 5(b), the  $H_C$  increases as the sample thickness decreases and reaches 8200 Oe at 4 ML. This increase in coercivity is probably due to the increase in shape anisotropy originating from magnetostatic or dipole interactions.<sup>41</sup>

In summary, a series of CrTe<sub>2</sub> thin films with various thicknesses have been synthesized by MBE. All the films show strong ferromagnetism with an out-of-plane easy axis. More importantly, as the film thickness decreases from 35 to 4 ML, the Curie temperature decreases only slightly from 205 to 191 K, while the coercive field ( $H_C$ ) increases from 5120 to 8200 Oe. With distinct magnetic properties, large area CrTe<sub>2</sub> thin films grown by MBE are promising for stacking with other 2D materials and suitable for all van der Waals material electronic devices.

See the [supplementary material](#) for RHEED patterns of the CrTe<sub>2</sub> thin films with different thicknesses, RHEED intensity oscillations during growth, x-ray diffraction methods to calculate the lattice parameter  $c$ , and  $R_{AHE}$  of all the CrTe<sub>2</sub> films vs magnetic field at various temperatures.

This work was supported by the National Key Research and Development Program of China (Grant Nos. 2016YFA0300803 and 2017YFA0206304), the National Natural Science Foundation of China (Grant Nos. 61474061, 61674079, 61974061, and 61805116), the Natural Science Foundation of Jiangsu Province of China (Grant Nos. BK20180056 and BK20200307), and the China Postdoctoral Science Foundation, China (Grant No. 2019M661787).

## DATA AVAILABILITY

The data that support the findings of this study are available from the corresponding author upon reasonable request.

## REFERENCES

- <sup>1</sup>W. Han, R. K. Kawakami, M. Gmitra, and J. Fabian, *Nat. Nanotechnol.* **9**(10), 794–807 (2014).
- <sup>2</sup>Z. Lin, Y. Liu, U. Halim, M. Ding, Y. Liu, Y. Wang, C. Jia, P. Chen, X. Duan, and C. Wang, F. Song, M. Li, C. Wan, Y. Huang, and X. Duan, *Nature* **562**(7726), 254–258 (2018).
- <sup>3</sup>D. Akinwande, N. Petrone, and J. Hone, *Nat. Commun.* **5**(1), 5678 (2014).
- <sup>4</sup>Q. H. Wang, K. Kalantar-Zadeh, A. Kis, J. N. Coleman, and M. S. Strano, *Nat. Nanotechnol.* **7**(11), 699–712 (2012).
- <sup>5</sup>K. F. Mak and J. Shan, *Nat. Photonics* **10**(4), 216–226 (2016).
- <sup>6</sup>B. W. H. Baugher, H. O. H. Churchill, Y. Yang, and P. Jarillo-Herrero, *Nat. Nanotechnol.* **9**, 262 (2014).
- <sup>7</sup>V. O. Yazyev, *Rep. Prog. Phys.* **73**(5), 056501 (2010).
- <sup>8</sup>G. Z. Magda, P. Vancsó, Z. Osváth, P. Nemes-Incze, and L. Biró, *Nature* **514**, 608 (2014).
- <sup>9</sup>D. Zhong, K. L. Seyler, X. Linpeng, R. Cheng, N. Sivadas, B. Huang, E. Schmidgall, T. Taniguchi, K. Watanabe, and M. A. McGuire, *Sci. Adv.* **3**(5), e1603113 (2017).
- <sup>10</sup>S. Jiang, L. Li, Z. Wang, K. F. Mak, and J. Shan, *Nat. Nanotechnol.* **13**, 549 (2018).
- <sup>11</sup>Y. Deng, Y. Yu, Y. Song, J. Zhang, N. Z. Wang, Z. Sun, Y. Yi, Y. Z. Wu, S. Wu, and J. Zhu, *Nature* **563**, 94 (2018).
- <sup>12</sup>Z. Fei, B. Huang, P. Malinowski, W. Wang, T. Song, J. Sanchez, W. Yao, D. Xiao, X. Zhu, A. F. May, W. Wu, D. H. Cobden, J.-H. Chu, and X. Xu, *Nat. Mater.* **17**(9), 778–782 (2018).
- <sup>13</sup>M. Mogi, A. Tsukazaki, Y. Kaneko, R. Yoshimi, K. S. Takahashi, M. Kawasaki, and Y. Tokura, *APL Mater.* **6**(9), 091104 (2018).
- <sup>14</sup>H. Ohno, D. Chiba, F. Matsukura, T. Omiya, E. Abe, T. Dietl, Y. Ohno, and K. Ohtani, *Nature* **408**, 944 (2000).
- <sup>15</sup>B. Huang, G. Clark, E. Navarro-Moratalla, D. R. Klein, R. Cheng, K. L. Seyler, D. Zhong, E. Schmidgall, M. A. McGuire, and D. H. Cobden, *Nature* **546**, 270 (2017).
- <sup>16</sup>D. C. Freitas, R. Weht, A. Sulpice, G. Remenyi, and P. Strobel, F. Gay, J. Marcus, M. Núñez-Regueiro, *J. Phys.: Condens. Matter* **27**(17), 176002 (2015).

- <sup>17</sup>K. Lasek, P. M. Coelho, K. Zberecki, Y. Xin, and M. Batzill, *ACS Nano* **14**, 8473 (2020).
- <sup>18</sup>A. Purbawati, J. Coraux, J. Vogel, A. Hadj-Azzem and N. Rougemaille, *ACS Appl. Mater. Interfaces* **12**, 30702 (2020).
- <sup>19</sup>X. Sun, W. Li, X. Wang, Q. Sui, T. Zhang, Z. Wang, L. Liu, D. Li, S. Feng, S. Zhong, H. Wang, V. Bouchiat, M. Nunez Regueiro, N. Rougemaille, J. Coraux, A. Purbawati, A. Hadj-Azzem, Z. Wang, B. Dong, X. Wu, T. Yang, G. Yu, B. Wang, Z. Han, X. Han, and Z. Zhang, *Nano Res.* **13**, 3358–3363 (2020).
- <sup>20</sup>D. R. Klein, D. Macneill, J. L. Lado, D. Soriano, E. Navarro-Moratalla, K. Watanabe, T. Taniguchi, S. Manni, P. Canfield, J. Fernández-Rossier, and P. Jarillo-Herrero, *Science* **360**(6394), 1218–1222 (2018).
- <sup>21</sup>C. Gong, L. Li, Z. Li, H. Ji, A. Stern, Y. Xia, T. Cao, W. Bao, C. Wang, Y. Wang, Z. Q. Qiu, R. J. Cava, S. G. Louie, J. Xia, and X. Zhang, *Nature* **546**(7657), 265 (2017).
- <sup>22</sup>Y. Sun, M. Kanagaraj, Q. Gao, Y. Zhao, J. Ning, K. Zhang, X. Lu, L. He, and Y. Xu, *Chin. Phys. Lett.* **37**(7), 077501 (2020).
- <sup>23</sup>L. He, F. Xiu, Y. Wang, A. V. Fedorov, G. Huang, X. Kou, M. Lang, W. P. Beyermann, J. Zou, and K. L. Wang, *J. Appl. Phys.* **109**, 103702 (2011).
- <sup>24</sup>A. O. Fumega, J. S. Phillips, and V. Pardo, *J. Phys. Chem. C* **124**, 21047 (2020).
- <sup>25</sup>L. He, X. Kou, and K. L. Wang, *Phys. Status Solidi RRL* **7**, 50–63 (2013).
- <sup>26</sup>H. Y. Lv, W. J. Lu, D. F. Shao, Y. Liu, and Y. P. Sun, *Phys. Rev. B* **92**, 214419 (2015).
- <sup>27</sup>L. He, X. Kou, M. Lang, E. S. Choi, Y. Jiang, T. Nie, W. Jiang, Y. Fan, Y. Wang, F. Xiu, and K. L. Wang, *Sci. Rep.* **3**, 3406 (2013).
- <sup>28</sup>K. Wang, Y. Liu, W. Wang, N. Meyer, L. H. Bao, L. He, M. R. Lang, Z. G. Chen, X. Y. Che, K. Post, J. Zou, D. N. Basov, K. L. Wang, and F. Xiu, *Appl. Phys. Lett.* **103**(3), 031605–031604 (2013).
- <sup>29</sup>X. F. Kou, W. J. Jiang, M. R. Lang, F. X. Xiu, L. He, Y. Wang, Y. Wang, X. X. Yu, A. V. Fedorov, P. Zhang, and K. L. Wang, *J. Appl. Phys.* **112**(6), 063912 (2012).
- <sup>30</sup>F. Tsui, L. He, L. Ma, A. Tkachuk, Y. S. Chu, K. Nakajima, and T. Chikyow, *Phys. Rev. Lett.* **91**(17), 177203 (2003).
- <sup>31</sup>N. Nagaosa, J. Sinova, S. Onoda, A. H. Macdonald and N. P. Ong, *Rev. Mod. Phys.* **82**(2), 1539–1592 (2010).
- <sup>32</sup>W. Liu, D. West, L. He, Y. Xu, J. Liu, K. Wang, Y. Wang, G. van der Laan, R. Zhang, S. Zhang, and K. L. Wang, *ACS Nano* **9**(10), 10237–10243 (2015).
- <sup>33</sup>F. Cui, X. Zhao, J. Xu, B. Tang, Q. Shang, J. Shi, Y. Huan, J. Liao, Q. Chen, and Y. Hou, *Adv. Mater.* **32**(4), 1905896 (2020).
- <sup>34</sup>D. Zhang, A. Richardella, D. W. Rench, S. Y. Xu, and N. Samarth, *Phys. Rev. B* **86**(20), 205127 (2012).
- <sup>35</sup>A. Arrott, *Phys. Rev.* **108**(6), 1394–1396 (1957).
- <sup>36</sup>F. Matsukura, H. Ohno, A. Shen, and Y. Sugawara, *Phys. Rev. B* **57**(4), R2037 (1998).
- <sup>37</sup>I. Stuchnov, S. W. E. Riester, H. J. Trodahl, N. Setter, A. W. Rushforth, K. W. Edmonds, R. P. Campion, C. T. Foxon, B. L. Gallagher, and T. Jungwirth, *Nat. Mater.* **7**(6), 464–467 (2008).
- <sup>38</sup>J. Ning, Y. Zhao, Z. Chen, Y. Sun, Q. Gao, Y. Chen, M. Kanagaraj, J. Zhang, and L. He, *J. Phys. D: Appl. Phys.* **53**(50), 505001 (2020).
- <sup>39</sup>L. Bao, W. Wang, N. Meyer, Y. Liu, C. Zhang, K. Wang, P. Ai, and F. Xiu, *Sci. Rep.* **3**, 2391 (2013).
- <sup>40</sup>H. U. Jingshi and T. F. Rosenbaum, *Nat. Mater.* **7**(9), 697–700 (2008).
- <sup>41</sup>Y. Fujisawa, M. Pardo-Almanza, J. Garland, K. Yamagami, X. Zhu, X. Chen, K. Araki, T. Takeda, M. Kobayashi, Y. Takeda, C. H. Hsu, F. C. Chuang, R. Laskowski, K. H. Khoo, A. Soumyanarayanan, and Y. Okada, *Phys. Rev. Mater.* **4**(11), 114001 (2020).